Journal of Alloys and Compounds, 183 (1992) 288–302
JALCOM 7019

Magnetization and flux pinning studies of superconducting In–21.8at.%Bi eutectic alloys*

P. D. Currie†, T. R. Finlayson and T. F. Smith††
Department of Physics, Monash University, Clayton 3168 (Australia)

(Received July 3, 1991)

Abstract

Magnetization studies are described for In–21.8at.%Bi eutectic materials having both random ('as-cast') microstructures and well-aligned lamellae produced by directional solidification. Pinning forces are calculated from the magnetization curves and an adequate description for the random eutectic has been achieved using the Dew-Hughes model for 'magnetic–volume–normal' pinning. However, none of the conventional models for flux pinning fits the measured magnetization for the aligned lamellar microstructure for which a 'flux short-circuit' model is proposed. A feature of this model is a field H_1 below which the whole sample behaves like an homogeneous superconductor, but above which one set of normal lamellae provides pathways for unrestricted flux flow through the sample. This model also provides a consistent explanation for the flux pinning observed in the aligned eutectic material as a function of heat treatment.

1. Introduction

Flux pinning in the mixed state for type II superconductors has been reviewed in a number of articles [1–4]. Flux lines may become pinned by spatial variations in the free energy. Such variations are associated with crystal defects, second phases, voids, strain fields etc. An adequate understanding of flux pinning is provided by the critical state model [5] for which there is a maximum current density $J_c(B)$ which can be carried by a superconductor without loss. Locally within the $j_c(b)$ material, the superconductor carries a current that is either the critical current density appropriate to the local magnetic field or zero. A Lorentz force is exerted on flux lines through the current density, and in the critical state this may be equated to the pinning force $\boldsymbol{F}_p$ associated with metallurgical features in the material

$$\boldsymbol{F}_p = -\boldsymbol{J}_c \times \boldsymbol{B} \tag{1}$$

where $\boldsymbol{B}$ is the magnetic induction. Accordingly, $\boldsymbol{F}_p$ can be obtained from critical current measurements, and can also be derived from magnetization

*Dedicated to Professor W. Bronger and Professor Ch. J. Raub on the occasions of their 60th birthdays.

†Present address: 4 Chapel Court, Warwick, QLD 4370, Australia.
††Present address: Vice-Chancellor's Office, La Trobe University, Bundoora, Vic. 3083, Australia.

0925-8388/92/$5.00

vs. applied field curves [6]. For most materials studied to date

$$F_p = [H_{c2}(T)]^n f(b) \tag{2}$$

where n is close to 2.5 and $f(b)$ is a function only of b, the reduced inductance B/B_{c2}. As must follow from eqn. (1), F_p is zero at $b = 0$ and $b = 1$, and peaks at some intermediate value. Two independent models have used different assumptions regarding pinning mechanisms, to predict the functional form of $f(b)$.

Kramer [7] proposed that the peak in F_p corresponds to a changeover in the mechanism of flux motion from depinning to synchronous shear of the flux-line lattice (FLL) about pins too strong to be broken. Pinning strength is only moderate at low fields through the dominance of FLL elasticity, which limits relaxation of flux lines towards pinning sites. At high fields, $f(b)$ takes the form

$$f(b) = Kb^{1/2}(1-b)^2 \tag{3}$$

where K is a constant at a given temperature. The influence of specific pinning mechanisms shows up through the position of the peak. Weak or widely spaced pins result in a small peak near $b = 1$. Stronger pinning (which may be introduced in the same specimen by metallurgical treatment) shifts the peak in F_p to lower b values. Good agreement with experiment using data from the literature was reported by Kramer [7].

Dew-Hughes [8], however, considered a pinning force determined by the work done per unit length of flux line in unpinning. The pinning force per unit volume is then given by

$$F_p = -\eta L \Delta W / x \tag{4}$$

where ΔW is the work done in moving unit length of flux line from a pinning centre to the nearest position where it is unpinned, x is the effective range of the pinning interaction, L is the total length of flux line per unit volume that is directly pinned and η is an efficiency factor determined by the extent to which any one flux line can relax to a position of maximum pinning against the interaction of its neighbours in the FLL. For many real materials, effective pinning is by sites distributed densely but at random in three dimensions, making it unlikely that any element of the FLL could undergo shear without having to be first unpinned. Moreover, pinning forces in 'hard' type II superconductors are much stronger than interfluxoid forces, ensuring that the FLL will be sufficiently disrupted in the neighbourhood of pinning centres to allow maximum pinning, and FLL elasticity may be disregarded (*i.e.* $\eta = 1$). It is then possible to calculate the dependence of F_p on b, distinguishing various mechanisms by the following criteria.

(a) Pinning interactions are either 'magnetic' or 'core', implying that the size and spacing of pinning centres are either greater or less than the penetration depth λ. If these parameters are greater than λ, B adjusts everywhere to its equilibrium value and pinning occurs at the surface of the pinning sites through the existence of a 'Bean–Livingston surface barrier'

[9]. If either the size or the spacing of the pinning sites is less than λ, B must take an average value. Pinning is then effected via the different free energies of fluxoids in the pinning site and the matrix, owing to their different superconducting properties.

(b) Pinning sites are 'volume', 'surface' or 'point', depending on the number of their dimensions which are large compared with the interflux-line spacing ($d = 1.07\ (\phi_0/B)^{1/2}$ [9], where ϕ_0 is the flux quantum).

(c) Pinning is either 'normal' or '$\Delta\kappa$', according to whether the pinning sites consist of non-superconducting material (normal metal, insulator or void) or superconducting material of a different order parameter κ, usually produced by compositional fluctuations.

The various pinning functions and positions for maxima in these functions are given in Table 1.

A number of fundamental studies of flux pinning in type II superconductors has been undertaken using eutectic alloys [10–13] which are excellent model systems in that both the scale and the nature of the interlamellae boundaries can be systematically varied. The microstructure of In–21.8at.%Bi eutectic material consists of a terminal solid solution (α below 49 °C, α_1, between 49 and 72 °C) and a β phase (containing 32% Bi) [14]. (It should be noted that the most recent publication of the phase diagram for the In–Bi system [15] does not take account of the existence of the α_1 phase and the effect this has on the equilibrium phase diagram.) As-cast samples have random microstructures but a well-aligned lamellar morphology can be produced by directional solidification [10–12]. The aligned lamellar microstructure is highly sensitive to heat treatment, which has been attributed to the marked change in bismuth solubility in the α and α_1 phases between 20 and 70 °C, and because the $\alpha_1 \rightarrow \alpha$ transformation occurring at 49 °C (under pseudoequilibrium conditions) introduces strains, leading to fine-scale precipitation of β in the α phase [16].

TABLE 1

Field-dependent pinning functions and positions of maxima for the various mechanism combinations[a]

Type of interaction	Geometry of pin	Type of centre	Pinning function $F_p(b)$	Position of maximum
Magnetic	Volume	Normal	$b^{1/2}(1-b)$	$b=0.33$
		$\Delta\kappa$	$b^{1/2}(1-2b)$	$b=0.17,1$
Core	Volume	Normal	$(1-b)^2$	—
		$\Delta\kappa$	$b(1-b)$	$b=0.5$
	Surface	Normal	$b^{1/2}(1-b)^2$	$b=0.2$
		$\Delta\kappa$	$b^{3/2}(1-b)$	$b=0.6$
	Point	Normal	$b(1-b)^2$	$b=0.33$
		$\Delta\kappa$	$b^2(1-b)$	$b=0.67$

[a]After Dew-Hughes [8].

We report here the influence of microstructure on the magnetization behaviour of In–21.8at.%Bi. The pinning force functions of Dew-Hughes [8] are used to assess the operative pinning mechanisms. A 'flux short-circuit' model is proposed to explain the detailed shape of magnetization curves for the aligned microstructure. The results show the fundamental role played by microstructure in determining magnetic hysteresis in this material.

2. Experimental methods

The material of eutectic composition used for this investigation was prepared by melting together the constituent amounts of indium and bismuth of purity 99.999% in a sealed Pyrex® capsule, evacuated and backfilled to 10^{-3} Pa with high-purity argon. After mixing the liquid for several minutes, the melt was poured through a constriction at one end of the capsule and cast in the form of a rod 3.5 mm in diameter in a Pyrex tube attached to the capsule. The tube could then be separated from the capsule and the casting subsequently processed. This included directional solidification, as described elsewhere [12]. Typical optical micrographs showing the as-cast and directionally solidified structures are reproduced in Fig. 1.

Magnetization samples were spark cut to lengths of 33 mm from either as-cast or directionally solidified rods. Sample heat treatments were done either in a water bath, thermostatically controlled to ± 1.0 °C. for temperatures above room temperature, or in a commercial Hetofrig, for temperatures between room temperature and -40 °C. In each case the sample was placed in a Pyrex test tube which was maintained under a dynamic vacuum of approximately 10 Pa and which was immersed in the water bath or Hetofrig fluid, usually methanol.

Magnetization *vs.* applied magnetic field data were obtained using a vibrating-sample magnetometer, of the type described by Foner [17]. In general, for directionally solidified material, interlamellae boundaries lay parallel to the applied field. Additional measurements were carried out on

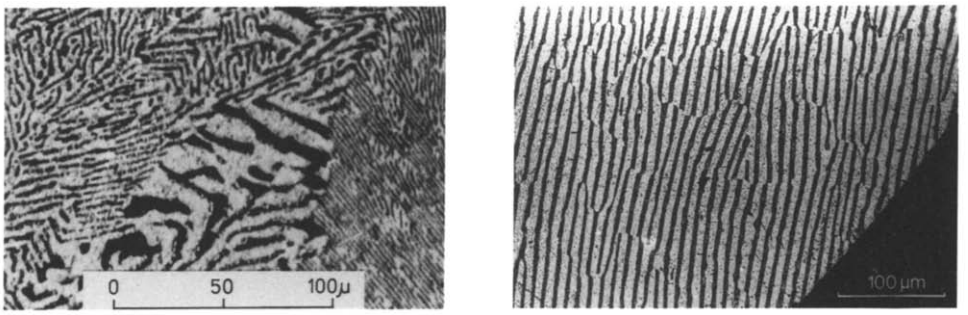

(a) (b)

Fig. 1. Optical micrographs from In–21.8at.%Bi eutectics, showing (a) as-cast and (b) directionally solidified microstructures. The dark regions are the α phase.

two small samples with dimensions $3\times3\times1$ mm^3, spark cut from a bulk sample, one parallel to the cylinder axis, the other normal to the axis. Using the latter, magnetization was recorded with the applied field normal to the interlamellar boundaries.

3. Results

The magnetization curve of a sample with as-cast microstructure is shown in Fig. 2. F_p *vs.* b, calculated from Fig. 2, is compared in Fig. 3 with the Dew-Hughes function corresponding to 'magnetic–volume–normal' pinning. Agreement is good, particularly in regard to the position of the peak. F_p was calculated from magnetization data following Lange [6]:

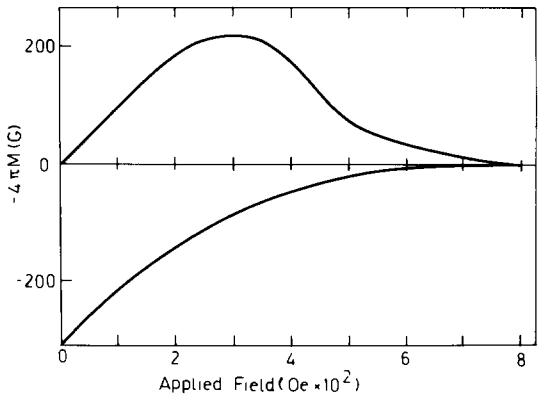

Fig. 2. Magnetization curve for In–21.8at.%Bi eutectic alloy with as-cast random lamellar microstructure.

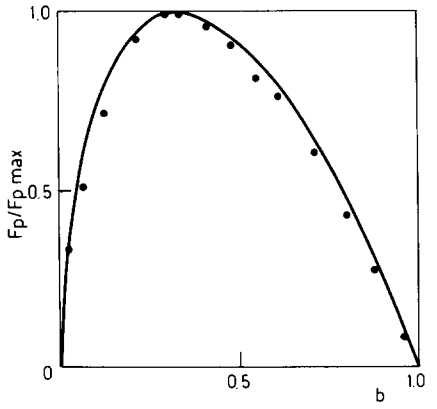

Fig. 3. Pinning force *vs.* reduced induction for an as-cast eutectic sample, aged for 1 month at room temperature: $b^{1/2}(1-b)$ ——, the Dew-Hughes pinning function for 'magnetic–volume–normal' pinning. The data are typical of all eutectic samples with random microstructures.

$$F_p(B) = BJ_c(B) = \frac{3 + 4\pi M'}{1 + 4\pi M'} \frac{4\pi M}{R} B \tag{5}$$

where M' is the slope of the increasing-field magnetization curve at a given induction B, and R is the radius of the cylindrical sample.

Preliminary magnetization results for aligned lamellar samples [12] showed that the different behaviours for the two component phases could be distinguished, owing to the appearance of a distinct hysteresis change near H_1, as illustrated in Fig. 4. H_1 and H_2 (the upper critical field) were linked with the upper critical fields of the two component phases, α and β, by the assignment of H_α and H_β, respectively, as in Fig. 5. The slope change at (50 ± 2 °C, 1.36 ± 0.02 kOe) in Fig. 5 can be attributed to the transformation $\alpha \rightarrow \alpha_1$ within the sample and H_{α_1} is labelled accordingly in Fig. 5. F_p *vs.* b data calculated from the magnetization curves for the aligned eutectic sample, following three different heat treatments, are shown in Fig. 6. The three cases are for the α phase normal above $b = 0.05$ (heat treatment temperature $T_h = 9$ °C), above $b = 0.42$ ($T_h = 30$ °C) and above $b = 0.95$ ($T_h = 40$ °C). It should be noted that all curves coincide, with suitable normalization. The curve for $T_h = 30$ °C changes by a scaling factor at $b = 0.42$, but its functional form is maintained. The dip at $b = 0.42$ corresponds approximately to the apparent critical field H_1, defined in Fig. 4. The common curve from Fig. 6 is then plotted, along with the Dew-Hughes pinning functions for which peaks lie nearest to the experimental peak, in Fig. 7. Intermediate behaviour between the Dew-Hughes functions is apparent.

Testing the effect of field orientation to the lamellae boundaries led to the magnetization curves of Fig. 8. Small samples with field parallel to and field normal to boundaries were measured, for comparison with the large

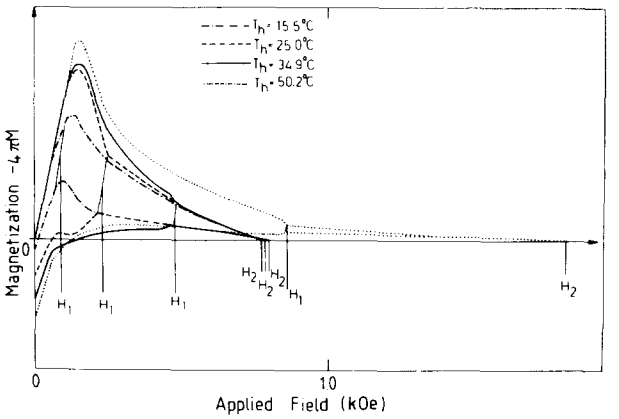

Fig. 4. Influence of heat treatment temperature T_h on magnetization of an aligned lamellar eutectic sample at 4.2 K: – · –, $T_h = 15.5$ °C; – – –, $T_h = 25.0$ °C; ——, $T_h = 34.9$ °C; · · ·, $T_h = 50.2$ °C. For each curve shown, H_1 is chosen as the midpoint of the line drawn to join the anomalous inflexions in the increasing- and decreasing-field segments of the curve. H_2 indicates the upper critical field of the sample in each case.

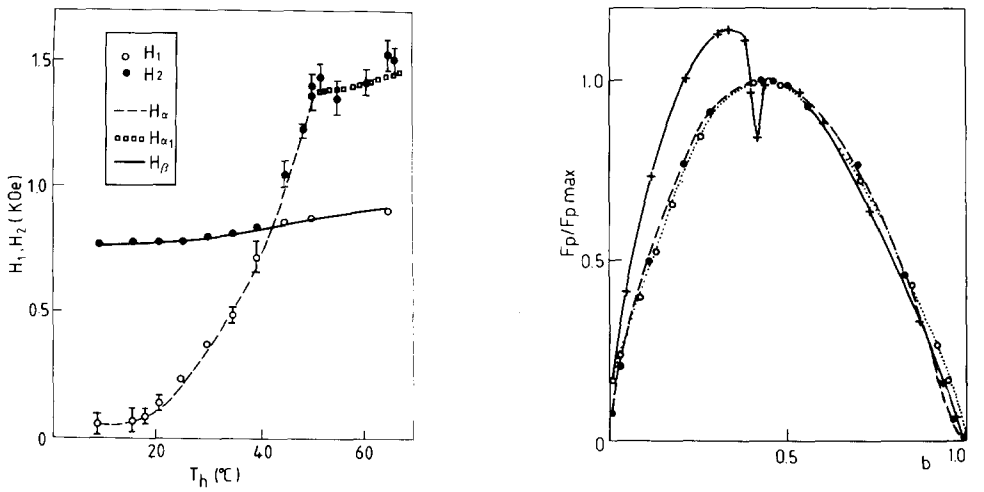

Fig. 5. H_1 (○) and H_1 (●) (as defined in Fig. 4) *vs.* heat treatment temperature. (All data are for T_h increasing except that for 48.5 °C): – – –, H_α; □, $H_{\alpha 1}$ (for heat treatment above 49 °C); ——, H_β.

Fig. 6. Pinning force curves for aligned eutectic samples after heat treatment at 9 °C (○), 30 °C (+) and 40 °C (●). The 30 °C curve has been scaled to normalize the $H > H_1$ data. If the same curve is scaled to normalize the $H < H_1$ data, the branch below the dip at $b = 0.42$ coincides with the other curves shown.

sample in parallel field. While there were minor changes in the overall shape of the magnetization curve for the small sample (field parallel to boundaries) by comparison with that for the regular magnetization sample, it is clear from comparisons of the overall hystereses and remanent magnetizations that pinning was stronger for the applied field parallel to the lamellae boundaries than for the perpendicular. The resultant pinning force data are plotted in Fig. 9.

Although the field parameters H_α and H_β, as shown in Fig. 5, were reversible with heat treatment temperature, under certain treatment sequences, the magnetic hysteresis was not reversible by reversing the heat treatment. Cycling T_h in the range 20–48.5 °C or between 50 and 66 °C left all features of the magnetization curves reversible. However, reduction from the latter range to the former introduced a significant increase in hysteresis. As shown in Fig. 10, the heat treatment sequence of 50.5 °C followed by 31 °C produced an increase in remanent induction B_r, of more than six times those for separate heat treatments at either 30 or 50.5 °C. However, B_r returned to its original value (close to B_{r1} in Fig. 10) within three months of sample storage at room temperature with 90% reduction of the excess ($B_{r3} - B_{r1}$ in Fig. 10) occurring in 25 days. It should be noted that the enhancement in magnetic hysteresis appears almost entirely below H_α. Although the data are not reproduced here, it was observed [18] that heat treatments at temperatures just below 0 °C following treatment at 50.5 °C also increased the low-field hysteresis and B_r, but only minutes at the lower heat treatment temperature

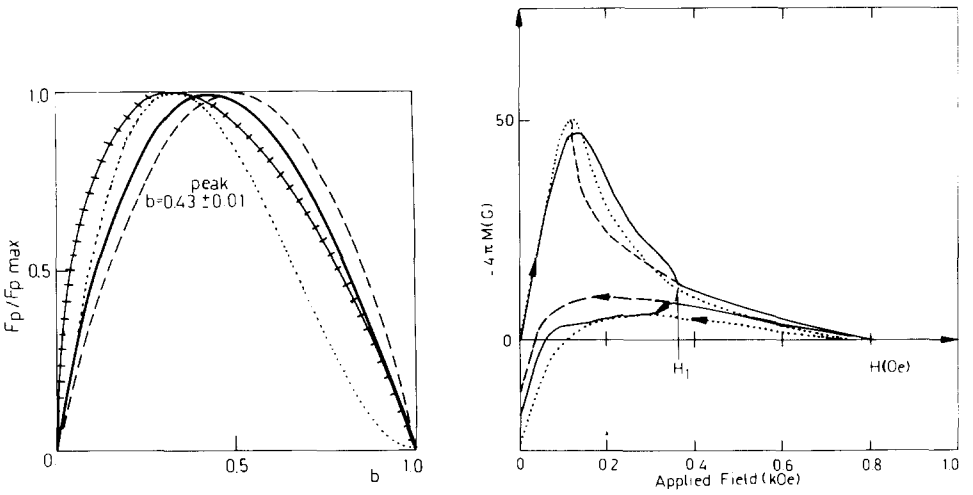

Fig. 7. The average pinning force (——) for the three different data sets in Fig. 6 (disregarding the unnormalized segment of the $T_h = 30$ °C curve): peak, $b = 0.43 \pm 0.01$. For comparison, the three pinning functions [8] with peaks near to that of the experimental curve are plotted: –+–+–+–, 'magnetic–volume–normal' pinning ($b^{1/2}(1-b)$); · · ·, 'core–point–normal' pinning ($b(1-b)^2$); – – –, 'core–volume–$\Delta\kappa$' pinning ($b(1-b)$).

Fig. 8. Magnetization curves measured at 4.2 K after heat treatment at 30 °C for In–21.8at.%Bi aligned lamellar eutectic in three specimen geometries: ——, regular magnetization specimen (33 mm×3.5 mm diameter cylinder), with lamellae boundaries parallel to applied field; · · ·, $1 \times 1 \times 3$ mm^3 specimen with lamellae parallel to applied field; – – –, $1 \times 1 \times 3$ mm^3 specimen with lamellae perpendicular to applied field. All three specimens were taken from the same directionally solidified ingot.

were required, whereas for the sequence 50.5 °C followed by 31 °C the change took place over about a 2 h period at 31 °C.

4. Discussion

4.1. Assessment of flux pinning using the Dew-Hughes model

The data in Fig. 3 indicate that the pinning mechanism operative in the as-cast eutectic is 'magnetic–volume–normal', in the terminology of Dew-Hughes [8]. This is consistent with the microstructure revealed by optical and scanning electron microscopy [16], for the following reasons.

(a) Both the separation and the size of α-phase particles exceed the penetration depth which at 4.2 K is in the range 0.04–0.4 μm for α or α_1 phases, and 0.1–0.16 μm for β phase [18], confirming the 'magnetic' nature of pinning.

(b) The criterion for 'volume' pinning is satisfied, since the dimensions of pinning sites (*i.e.* the α-phase particles) exceed the flux-line spacing which is 0.5 μm at $b = 0.1$ and less at higher inductions.

(c) The pinning sites are 'normal', since the upper critical field of the α phase, following room temperature ageing (the composition being In–4%Bi

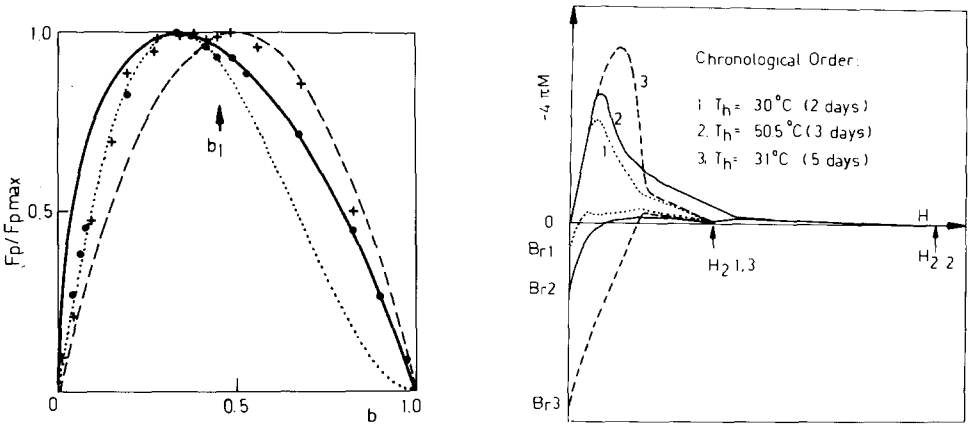

Fig. 9. Pinning force curves for small aligned lamellar eutectic magnetization samples after heat treatment at 30 °C, with lamellae boundaries parallel (●) or perpendicular (+) to the applied magnetic field. The two cases coincide below b_1 (the b value corresponding to H_1, as defined in Fig. 4), but diverge above. The three Dew-Hughes pinning functions plotted are for 'magnetic–volume–normal' pinning ($b^{1/2}(1-b)$) (——); 'core–point–normal' pinning ($b(1-b)^2$) (· · ·); 'core–volume–$\Delta\kappa$' pinning ($b(1-b)$) (– – –).

Fig. 10. Increased magnetic hysteresis in an In–21.8at.%Bi aligned lamellar eutectic sample, induced by the following heat treatment sequence (chronological order) involving reduction of T_h through 49.3 °C: curve 1, T_h=30 °C, 2 days; curve 2, T_h=50.5 °C, 3 days; curve 3, T_h=31 °C, 5 days. The increase in remanent trapped flux B_r by a factor of 6.5 between curves 1 and 3, should be noted.

[14]) is below the lower critical field of the composite (140 Oe and approximately 200 Oe respectively).

One can conclude, then, that the Dew-Hughes model gives meaningful results for the as-cast eutectic.

Data from the aligned eutectic material needs more careful examination than that for the as-cast sample, in order to test the applicability of the Dew-Hughes model. Comparison with the Dew-Hughes pinning functions in Fig. 7 indicates 'magnetic–volume–$\Delta\kappa$' pinning, with a very large $\Delta\kappa$ contribution (*i.e.* pinning sites close to the normal state). This assessment is based on the fact that the peak in F_p lies between the 'normal' curve peaks ($b \leqslant 0.33$) and $\Delta\kappa$ curve peaks ($b \geqslant 0.5$) [8]. The best fit to the data is obtained with the 'magnetic–volume–normal' pinning function above $b \approx 0.5$. What might then be termed 'magnetic–volume–large $\Delta\kappa$' pinning at first seems fairly reasonable for this material, in that it is very similar to the mechanism deduced for the random (as-cast) eutectic above. However, to explain the unexpected fact that a common pinning curve is found for all T_h, one or more of the following postulates must be accepted.

(a) The Dew-Hughes model does not apply, and therefore comparison with the Dew-Hughes functions is not meaningful.

(b) Pinning is primarily caused by microstructural features within each phase, rather than by the boundaries.

(c) Pinning occurs at interphase boundaries, but is not principally determined by the difference in bulk superconducting properties and is therefore not sensitive to heat treatment which alters the magnitude of this difference.

The following evidence supports (a) and (c), while (b) must be rejected.

Point (a) has been verified through the observation of field-history effects in the magnetization behaviour of the same samples [18]. These effects show that FLL elasticity is important at low fields, whereas the Dew-Hughes model is based on the assumption that FLL elasticity can be ignored totally. Hence the model can apply only at high fields, if at all.

Explanation (b) above can be disregarded for three reasons. Firstly, Fig. 8 shows that pinning was stronger when the applied field was parallel to the lamellae boundaries. Figure 9 shows a correspondingly significant difference in the pinning function $F_p(b)$ above $b \approx 0.5$. The difference between these cases is the degree to which flux lines must change the fraction of their length situated in each phase in order to move. In the parallel case, flux lines may shift from one phase entirely into the other, while the normal case will involve only smaller changes related to irregularities in the interphase boundaries, local fluctuations in the proportions between the phases, lamellae terminations and other such minor microstructural imperfections. If pinning were due to microstructural features dispersed isotropically within one or both phases, no marked difference in hysteresis could be expected between the parallel- and normal-field cases. Since a clear discrepancy is seen in Fig. 8, the results support pinning by the difference between phases, *i.e.* at the interphase boundaries. Secondly, field-history-effect observations [18] show that at high fields the influence of FLL elasticity is reduced by strong pinning at lamellae boundaries.

Such conditions will be nearer to satisfying the assumptions of the Dew-Hughes model, and therefore the agreement between the data and the 'magnetic–volume–normal' pinning curve at high inductions in Fig. 7 may be meaningful. This pinning type has already been explained to be consistent with pinning at the interphase boundaries. Finally, a significant number of lamellae terminations are seen in the optical micrograph (Fig. 1) of the directionally solidified eutectic sample, preventing complete connectivity of each phase. This means that flux lines must cross interphase boundaries. Pinning at these boundaries must be fairly strong because of the large difference in superconducting properties across them. For this reason, it is likely that boundary pinning will be a major, if not predominant, mechanism for flux pinning in the aligned eutectic.

Point (c) above—that pinning at interphase boundaries is not primarily determined by heat treatment—seems necessarily to hold, from Fig. 7. Whether or not the Dew-Hughes model applies, one would expect the differences in magnitude of the discontinuity of superconducting parameters across the boundaries at the various T_h values to be reflected in changes to the F_p *vs.* b curve. After all, the boundary is a normal–superconducting boundary above $b \approx 0.15$ for $T_h = 9$ °C, but separates two superconductors for $T_h = 40$ °C. It

may be that the pinning strength of the boundary is generated mainly by stress fields introduced through differential thermal contraction during quenching. The compositional changes induced by heat treatment may then only appear in the form of the slight differences apparent between the three sets of data in Fig. 6.

To summarize the findings for the aligned samples, the pinning models of Dew-Hughes [8] cannot be applied to explain the results, except perhaps as a rough approximation when $b \approx 1$. Pinning occurs at interphase boundaries. However, pinning strength is not sensitive to the degree of dissimilarity between the superconducting properties of the two phases. This could be explained by strains set up at interphase boundaries by differential thermal contraction, dominating the flux-pinning process.

4.2. The 'flux short-circuit' model

The above discussion shows the need for a new approach to modelling the pinning of flux penetration and pinning in this highly aligned two-phase superconductor. Such a model must also be able to explain several other observations. Figures 11 and 12 show that the magnetization of the aligned lamellar eutectic sample was not simply the sum of the magnetizations of its two component phases acting independently. In fact, Fig. 12 closely

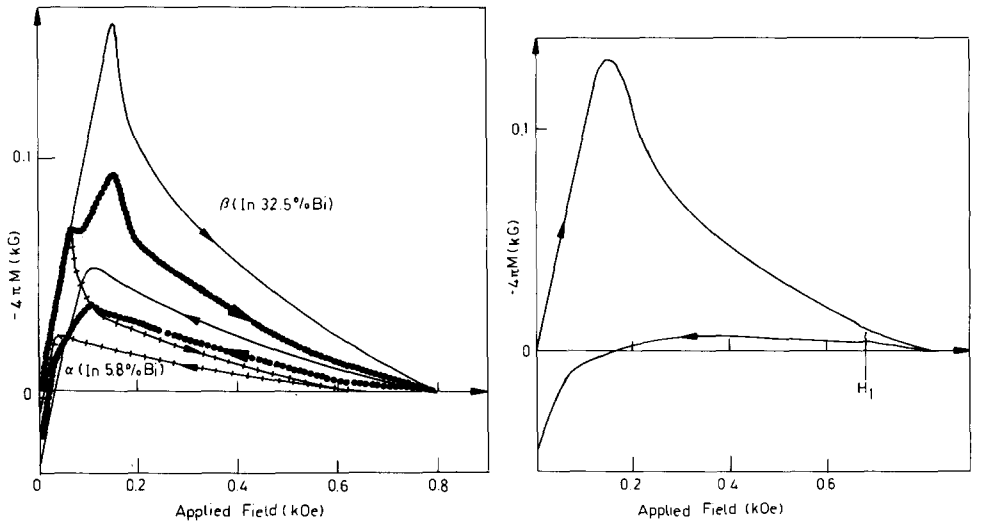

Fig. 11. Predicted magnetization curve (●●●) for the $\alpha-\beta$ eutectic sample, heat treated at 37 °C, based on a simple averaging of experimental magnetizations for α (In–5.8%Bi) (–+–+–+) and β (In–32.5%Bi) (——) phases. Single-phase alloy compositions have been chosen to match the component phases in an $\alpha-\beta$ eutectic held at 37 °C, from the In–Bi phase diagram [14].

Fig. 12. Experimental magnetization curve for the α–β aligned lamellar eutectic sample, heat treated for 4 days at 39.5 ± 1 °C. Comparison with the dotted curve in Fig. 11 shows marked differences, notably the greater hysteresis and the lack of double peaks below 0.3 kOe. The position of H_1 is consistent with the α-phase H_{c2} in Fig. 11, allowing for the difference in heat treatment temperatures.

resembles the behaviour of a conventional homogeneous superconductor, except for the feature near H_1. Figure 4 shows that this feature is not caused solely by the properties of one component phase, because hysteresis reduces irrespective of which phase, α or β, becomes normal. Nor is it likely to result from a change in pinning strength of the interphase boundaries. If that were so, one would expect a peak in hysteresis at H_1, of the type seen by Livingston [19], corresponding to the difference in superconducting parameters across the boundaries, passing through a maximum as one phase goes normal.

A simple model based on geometrical considerations can be used to describe what happens within the specimen at H_1. Essentially, the feature near H_1 signifies the existence, above H_1, of pathways for unimpeded flux flow via 'flux short circuits', reaching into all parts of the specimen, and consisting of material which has entered the normal state. Below H_1, the whole sample behaves in the same manner as an homogeneous superconductor. These stages of the magnetization process are depicted in Fig. 13 for increasing applied field. The figure shows schematically the microstructure of an aligned lamellar eutectic sample which in transverse section reveals some loss of connectivity in each phase, owing to lamellae terminations, mismatch boundaries, grain boundaries and such like. (The detailed microstructure and its variation with heat treatment are discussed elsewhere [16].) Associated with these microstructural sketches are plots of the average value of induction B_{av} as it varies with distance from the specimen centre. It should be emphasized that these plots are not 'flux profiles' in the usual sense [3] of showing the exact variation of B along any real straight path through the specimen centre.

At $H=H_A$ ($<H_1$) in Fig. 13, the sample is behaving as a near-homogeneous superconductor. The variation of B_{av} through the specimen resembles the familiar flux profile applicable to a conventional single-phase superconductor in which there is only one, simple, pinning mechanism. In this case, pinning probably occurs both at lamellae boundaries and within each phase, and small local variations of B will be found, particularly between the phases. The net behaviour is as illustrated. At $H=H_B$($>H_1$) flux has penetrated the α phase completely, leading to B_{av} in the α phase being equal to the applied induction value B_{app} in all parts of the sample. Flux has also penetrated further into the β phase because the applied field now has access to all β lamellae at their boundaries with the α phase, as well as at the specimen surface. β material is still superconducting, so that the variation of B_{av} with distance from the specimen centre is no longer identical in each phase, as it was at $H=H_A$. It is the penetration of B in this way into a large fraction of the sample within the field interval between H_A and H_B which produces the marked drop in (negative) magnetization near H_1, evident in the inset to Fig. 13. It should be noted that this model makes it unnecessary to postulate a sudden change in pinning strength within a macroscopically homogeneous material to explain the feature near H_1.

The transition from the state illustrated in Fig. 13 at $H=H_A$ to that at $H=H_B$ can be understood as follows. When the applied field reaches H_{c2}

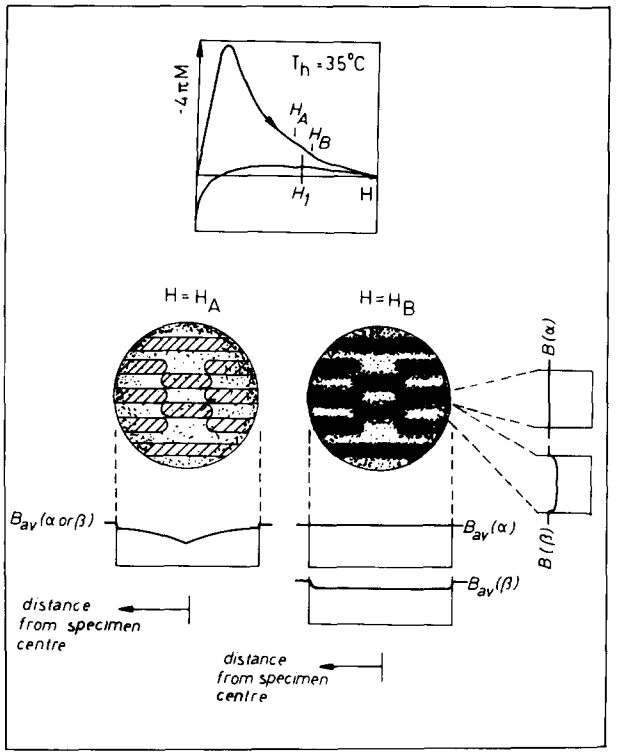

Fig. 13. Schematic diagram depicting flux distribution in a transverse section of an aligned lamellar eutectic sample, in the field-increasing regime, following heat treatment at 35 °C. The schematic microstructure illustrates loss of connectivity of each phase, away from the specimen surface, owing to lamellae imperfections and grain boundaries. The dot density signifies flux density (field out of page). The plots of flux density describe the average B in all parts of the sample (one or both phases included) located an equal distance from the specimen centre. These plots are not 'flux profiles', except in the case of those across lamellae widths at the right of the figure for $H=H_B$. For description of the process, see text.

for the α phase, flux penetrates those α lamellae which terminate at the surface, allowing immediate penetration of the applied field into the interior of the specimen. Only small increases in H_{app} are then required to drive neighbouring but unconnected α-phase lamellae normal. By this means the complete penetration of the α phase will take place over a relatively small range of applied field, which is reflected in the narrowness of the magnetization anomaly near H_1.

Referring now to the decreasing-field branch of the magnetization curve in Fig. 13, the form of the curve near H_1 can readily be understood from the above argument. Transition of α lamellae into the superconducting state eliminates their function as flux short circuits and thereafter flux flow will be limited by pinning within each phase. Hysteresis must increase, as observed. The finite width of the anomaly near H_1 in this case corresponds to re-creation of the effective 'flux profile' depicted in Fig. 13 for $H=H_A$, and

results from the lack of complete connectivity of each phase, just as for the field-increasing case.

From Fig. 4 it can be seen that a very similar feature was seen near H_1 for all T_h values except $T_h = 15.5$ °C. However, the fact that hysteresis is less, rather than greater, at fields below H_1, for $T_h = 15.5$ °C is consistent with the flux short-circuit model. Referring to the magnetization curve following this heat treatment it can be seen that, in the vicinity of H_1 along the field-decreasing curve, B is changing very little, and is almost zero. Removal of flux short circuits near H_1 does not substantially alter the amount of flux trapped in the specimen between H_1 and zero field.

Varying the orientation of the applied field to the eutectic lamellae yields data consistent with the flux short-circuit model. In Fig. 8, a small sample with lamellae parallel to the field shows a significant change of slope near H_1 as defined for the bulk sample, but another small specimen, with lamellae normal to the field, shows a much smaller feature. The former has the same experimental geometry as described above for bulk samples. In the latter case, α lamellae in the normal state may reduce the pinning strength of the material somewhat, by eliminating pinning of the fraction of each flux line which lies in that phase, but they cannot provide short-circuit paths for flux movement.

The application of the above model also highlights the degree of perfection of the aligned lamellar eutectic microstructure, such that the entire sample is 'short circuited' over a small range of applied fields. One can easily understand why no feature comparable with that near H_1 for an aligned sample is observed in the magnetization of the as-cast eutectic material. Presumably the necessity for microstructural perfection has prevented the observation of such a feature in previous studies of directionally solidified samples [10], where the absence of distinct magnetization behaviour attributable to the two phases has been interpreted as evidence for the operation of proximity effects. At the same time the occurrence of the anomaly near H_1 over a finite range of fields is taken as evidence for some imperfection in the lamellar microstructure, which prevents complete connectivity throughout the sample along each lamella. Pinning at interphase boundaries results from these imperfections.

The significant influence on the magnetization following heat treatment near 30 °C, of an intermediate treatment at 50 °C or above, as illustrated in Fig. 10, can also be understood. As will be shown elsewhere [16], the intermediate heat treatment gives rise to fine β precipitates in the α lamellae, nucleated at imperfections caused by strains associated with the $\alpha_1 \rightarrow \alpha$ phase transformation [14]. Such precipitates remain microstructurally stable with the further heat treatment at 31 °C and are the source of enhanced, low-field, flux pinning. The magnetization hysteresis is largely unaffected above H_1 since, in that field range, the α-phase lamellae are entirely normal. The observed slow reduction of the low-field hysteresis towards its initial value for $T_h = 30$ °C, over approximately 1 month, occurs on account of the coarsening of the β precipitates within the α-phase lamellae [16].

5. Conclusions

For In–21.8at.%Bi eutectic alloys with random (as-cast) lamellar microstructures, magnetic flux pinning can be described adequately by the pinning function given by Dew-Hughes [8] for 'magnetic–volume–normal' pinning in which the operative aspects of the microstructure are interphase boundaries.

For well-aligned (directionally solidified) lamellar microstructures of the same alloy composition, the model of Dew-Hughes is inadequate except perhaps at high fields, on account of field-history effects at low fields which arise on account of FLL elasticity.

A 'flux short-circuit' model, in which there is unrestricted flux flow through all lamellae in the normal state, is proposed. A parameter which is critical to the model is the field H_1, at which one of the lamellar phases becomes normal. Below this field the aligned eutectic behaves as a homogeneous superconductor. A universal pinning curve can describe the magnetization for all heat treatments, indicating the relevance of the morphology of the boundaries for flux pinning and not the difference in superconducting properties between the phases separated by the boundary. Above H_1, unrestricted flux flow through all lamellae of the normal phase takes place and the existence of the anomaly near H_1 attests to the degree of perfection within the alignment of the lamellae.

References

1 J. D. Livingston and H. W. Schadler, *Prog. Mater. Sci.*, *12* (1964) 185.
2 D. Dew-Hughes, *Rep. Prog. Phys.*, *34* (1971) 821.
3 A. M. Campbell and J. E. Evetts, *Adv. Phys.*, *21* (1972) 199.
4 P. Chaddah, *Pramana*, *36* (1991) 353.
5 C. P. Bean, *Rev. Mod. Phys.*, *36* (1964) 31.
6 F. Lange, *J. Low Temp. Phys.*, *17* (1974) 65.
7 E. J. Kramer, *J. Appl. Phys.*, *44* (1973) 1360.
8 D. Dew-Hughes, *Philos. Mag.*, *30* (1974) 293.
9 A. M. Campbell, J. E. Evetts and D. Dew-Hughes, *Philos. Mag.*, *18* (1968) 313.
10 J. E. Goodfellow, *Thesis*, University of Warwick, Coventry, 1969.
11 J. M. Dupart, R. A. Brand, J. Baixeras and O. Bethoux, *J. Phys. (Paris)*, *38* (1977) 393.
12 P. D. Currie, T. R. Finlayson and W. A. Rachinger, *Scripta Metall.*, *11* (1977) 59.
13 J. D. Klump, M. P. Zaitlin and J. D. Verhoeven, *Phys. Rev. B*, *26* (1982) 3639.
14 P. D. Currie, T. R. Finlayson and T. F. Smith, *J. Less-Common Met.*, *62* (1978) 13.
15 T. B. Massalaski, J. L. Murray, L. H. Bennett and H. Baker (eds.), *Binary Alloy Phase Diagrams*, Vol. 1, American Society for Metals, Metals Park, OH, 1986, p. 510.
16 P. D. Currie and T. R. Finlayson, in preparation.
17 S. Foner, *Rev. Sci. Instrum.*, *30* (1959) 548.
18 P. D. Currie, *Thesis*, Monash University, Clayton, Vic., 1978.
19 J. D. Livingston, *Appl. Phys. Lett.*, *8* (1966) 319.